AD-A173 084 DYNAMIC FRACTURE INITIATION AND PROPAGATION IN 4340 STEEL UNDER IMPACT LO..(U) CALIFORNIA INST OF TECH PASADENA GRADUATE AERONAUTICAL LABS A T ZEHNDER ET AL. 1/1

UNCLASSIFIED 1986 GALCIT-SM-86-6 N00014-85-K-0596 F/G 11/6 NL

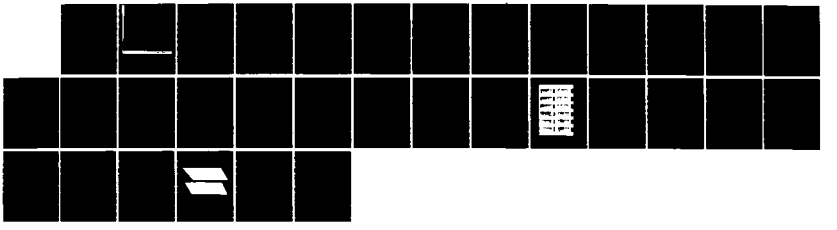

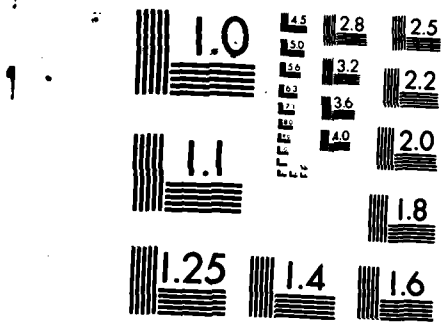

(4)

DYNAMIC FRACTURE INITIATION AND PROPAGATION IN 4340 STEEL UNDER IMPACT LOADING

by

Alan T. Zehnder* and Ares J. Rosakis**

CALIFORNIA INSTITUTE OF TECHNOLOGY

86 10 6 120

SM Report 86-6

DYNAMIC FRACTURE INITIATION AND PROPAGATION IN 4340 STEEL UNDER IMPACT LOADING

by

Alan T. Zehnder* and Ares J. Rosakis**

Graduate Aeronautical Laboratories

California Institute of Technology

Pasadena, CA 91125

* Graduate Research Assistant

** Assistant Professor of Aeronautics and Applied Mechanics

ABSTRACT

Dynamic fracture initation and propagation in 4340 steel was investigated experimentally using the optical method of reflected caustics combined with high speed photography. A new crack propagation testing configuration consisting of a three point bend specimen loaded in a drop weight tower was used. It was found that prior to crack initation the stress intensity factor time record calculated using the dynamic tup load and a static formula disagrees with the actual stress intensity factor measured by caustics. During crack propagation, the crack tip velocity and stress intensity factor time records varied smoothly and repeatably allowing for a straightforward interpretation of the data. The experiments show that for the particular heat treatment of 4340 steel used, the dynamic fracture propagation toughness depends on crack tip velocity through a relation that is a material property.

Key Words: Dynamic fracture initiation, dynamic crack propagation, caustics, 4340 steel, high-speed camera, stress-intensity factor, three point bend specimen.

1. INTRODUCTION

For dynamic crack propagation under conditions of small scale yielding, fracture criteria based on the stress intensity factor are expressed in a manner analogous to static fracture. This is done by introducing $K^d_I(t)$, the amplitude of the dynamic, asymptotic crack tip stress field [1] and a critical value K^d_{Ic}, which is usually assumed to be a material property. The quantity K^d_{Ic} represents the resistance of the material to crack growth and its magnitude is expected to depend on crack speed and on properties of the material.

The fracture propagation criterion is assumed to be

$$K^d_I[a(t),\dot{a}(t),t,Load] = K^d_{Ic}(\dot{a}(t)) \tag{1}$$

where a, and $\dot{a}$ are the crack length and crack tip velocity and t is time. This hypothesis states that setting the stress intensity factor, K_I^d, equal to the material's dynamic fracture toughness, K_{Ic}^d, determines an equation of motion for the crack length a(t). All inertial, plasticity and rate effects are lumped into the material property K_{Ic}^d thus simplifying the above hypothesis.

In principle K_I^d may be determined by a purely elastodynamic analysis. However K_{Ic}^d cannot be determined by analysis and thus must be determined by experiment or by micromechanical modelling of the dynamic fracture process [2]. In practice even K_I^d cannot generally be determined analytically. Thus numerical and optical techniques are necessary to interpret dynamic fracture experiments. The goal of such experiments is to determine whether the fracture toughness K_{Ic}^d can be safely considered a unique function of crack tip velocity and material properties. This question is still a subject of considerable discussion.

The available experimental results for dynamic crack propagation in metals are very limited. Several investigators [3-5] have used combined experimental and numerical techniques in which the boundary conditions applied to the specimen are measured (or assumed), and the crack length versus time is measured. These measurements are used in conjunction with a dynamic numerical model to calculate $K_I^d(t)$. Direct optical measurements using caustics or photoelasticity, combined with high speed photography, have been used extensively for investigating crack growth in transparent materials [6-8]. However, few direct optical measurements have been performed on metallic fracture specimens. Photoelastic coatings [9] and the method of reflected caustics [10] have been used to study crack growth in double cantilever beam specimens of 4340 steel. In both cases high dynamic effects due to reflected stress waves were present. Such effects are more pronounced in metallic specimens [11] and complicate the interpretation of experimental results. Thus no definitive statements regarding the existence of a unique K_{Ic}^d vs. $\dot{a}$ relation have yet been made for metals.

A1

In this paper dynamic fracture initiation and propagation experiments using the method of caustics are described. A new configuration for crack propagation experiments is used. This configuration, consisting of a three point bend specimen loaded in a drop weight tower, was found to produce repeatable and reliable results without the problems caused by the strong dynamic effects present when testing wedge loaded double cantilever beam specimens.

2. THE METHOD OF CAUSTICS

The discussion that follows describes reflected caustics, used for testing opaque materials, but with minor modifications the discussion holds for transmitted caustics, used for testing transparent materials.

Consider a set of parallel light rays normally incident on a planar, reflective specimen. Due to the crack tip loading the initially optically flat specimen is deformed into a shape such that the virtual extension of the reflected light rays forms an envelope in space as illustrated in Fig. 1. This surface, called the "caustic surface" is the locus of points of maximum luminosity. Its intersection with a reference plane located a distance z_o behind the specimen surface is the "caustic curve," a bright curve that bounds a dark region or shadow spot.

Suppose that light reflected from a point (x_1,x_2) on the specimen intersects a point (X_1,X_2) on the reference plane, where (x_1,x_2) is a coordinate system centered on the crack tip and (X_1,X_2) is an identical system on the reference plane. Then (X_1,X_2) are given by [12,13]

$$X_\alpha = x_\alpha - 2z_o \frac{\partial f(x_1,x_2)}{\partial x_\alpha} \tag{2}$$

where α ranges from 1 to 2, and $f(x_1,x_2) = -u_3(x_1,x_2)$, the out of plane surface displacement of the specimen. A caustic curve will exist if the Jacobian determinant of the map-

ping, Eq. (2), vanishes,

$$J(x_1,x_2,z_o) = \det\left[\frac{\partial X_\alpha}{\partial x_\beta}\right] = 0. \tag{3}$$

The set of points on the specimen such that J=0 forms a curve surrounding the crack tip called the "initial curve." The significance of the initial curve is that all points on this curve map directly onto the caustic curve.

By substituting the asymptotic, plane-stress u_3 displacement field [14] for a dynamically propagating crack into Eqs. (2) and (3) one can determine the shape of the caustic and can relate K_I^d to the caustic diameter D (width of the caustic in the direction perpendicular to the crack line). The relation is given by [10]

$$K_I^d = F(\dot{a})\,\frac{ED^{5/2}}{10.7 z_o \nu h}, \tag{4}$$

where

$$F(\dot{a}) = \frac{4\alpha_l\alpha_s-(1+\alpha_s^2)^2\,C(\alpha_l)}{(1+\alpha_s^2)(\alpha_s^2-\alpha_l^2)}, \tag{5}$$

$$C(\alpha_l) = \frac{(6.8+14.4\alpha_l-2.6\alpha_l^2)}{18.6}, \tag{6}$$

$$\alpha_{l,s} = \left[1-(\frac{\dot{a}}{C_{l,s}})^2\right]^{1/2}, \tag{7}$$

$\dot{a}$ is the crack speed, C_l and C_s are the longitudinal and shear wave speeds, E is Young's Modulus, ν is Poisson's Ratio and h is the specimen thickness. The initial curve is very nearly circular and its radius is closely approximated by [6]

$$r_o = F(\dot{a})^{-2/5}\ r_o^{stat} \tag{8}$$

where r_o^{stat} is the radius of the initial curve for stationary cracks given by

$$r_o^{stat} = .316D = \left\{\frac{3h\nu K_I z_o}{2\sqrt{2\pi}E}\right\}^{2/5}. \tag{9}$$

As $\dot{a}\rightarrow 0$ Eqs. (4) and (8) reduce to the caustics equations for stationary cracks.

Plane stress is a key assumption in the analysis of caustics. It is known [15] that due to the three-dimensional nature of the near crack tip field, the initial curve radius r_o must satisfy $r_o > 0.5h$, where h is the specimen thickness, for the plane-stress analysis of caustics to be accurate. Figure 2 shows the error for stationary cracks in K_I^{EXP} as measured with reflected caustics due to three-dimensional effects when $r_o < 0.5h$. Equation 9 shows that $r_o \sim (K_I z_o)^{2/5}$. The value of z_o was chosen and set prior to each experiment. Since K_I was initially zero, it is seen that $r_o > 0.5h$ could not always be satisfied during the loading. Thus the curve of Fig. 2 was used as a correction for calculating K_I when $r_o < 0.5h$. Once the crack started to propagate the value of K_I^d was always high enough to ensure $r_o > 0.5h$ for the prechosen value of z_o.

3. DESCRIPTION OF EXPERIMENTS

The experimental apparatus, consisting of a drop weight tower, digital recording oscilloscope, pulsed laser, and high speed camera is sketched in Fig. 3.

The specimen size was 30.4 × 12.8 × 0.95 cm with an initial crack length of 3.73 cm. The crack tip notch diameter was 0.3 mm for specimens 36, 37, and 39, and 1.4 mm for specimens 33, 34, and 38. The material composition and properties are given in Table 1. One surface of the specimen was ground, lapped, polished to a mirror finish, and vacuum coated with aluminum. The aluminum coating is an optional step but it increases the reflectivity by 50%.

The test specimens were dynamically loaded in 3-point bending by a Dynatup 8100A drop weight tester. The drop weight is variable, from 1910 N to 4220 N (430 lb-950 lb) and the maximum impact velocity is 10 m/s (32 ft/s) In the present experiments the weight was

1910 N and the velocity was 5.0 m/s. The tup (impact hammer) is instrumented allowing the dynamic impact force to be recorded on a Nicolet 2090 digital oscilloscope.

Two LED-Photodiode switches mounted on the drop weight tower provide trigger signals for the camera and oscilloscope. A flag mounted on the falling weight interrupts the light going from the LED to the photodiode causing a trigger pulse. One switch is positioned so that it triggers when the tup hits the specimen. This signal triggers the oscilloscope and the pulsing of the laser. The camera's mechanical capping shutter must be open before the impact, thus a second switch is mounted higher on the tower to provide a trigger 20 ms before impact.

The rotating mirror high speed camera can record 200 frames at up to 200,000 frames per second. Although it operates as a streak camera, discreet frames are obtained by pulsing the laser light source. Due to the short pulse width of the laser the exposure time of each frame is very short (15 ns), resulting in sharp photographs.

To photograph the caustics the camera is placed in front of the specimen to collect the reflected light and then focused at a distance z_o behind the specimen, i.e., focused on the reference plane of Fig. 1. Selected photographs obtained from a single test are shown in Fig. 4. The area covered by each frame is approximately 3 $cm \times 9$ cm. The bright curve surrounding each shadow spot is the caustic curve. Taking the moment of impact as 0 μs, it is seen that from 42 μs to 252 μs the shadow spot grew indicating that K_I was increasing. At 259 μs the crack began to propagate. The shadow spot moves with the crack tip, thus by measuring the location of the shadow spot the crack length may be determined. As the crack propagates it leaves behind a wake of plastic deformation causing the tail-like shadow patterns seen in the figure.

4. DYNAMIC CRACK INITIATION

Instrumented drop weight testing can be used to determine the energy absorbed by a material prior to fracture or to determine the dynamic fracture initiation toughness K_{Ic}^{d}.

The records of two impact tests are shown in Figure 5. Specimen 34 had a crack tip diameter of 1.4 mm and specimen 36 had a diameter of 0.3 mm. The true stress intensity factors, measured from caustics are presented along with the stress intensity factors calculated by using the dynamic tup load P(t) in a statically derived formula [16]

$$K_I(t) = P(t)\frac{3S}{2w^{3/2}}\ f(a/w), \qquad \textit{where}\quad f(0.3) = 0.95, \tag{10}$$

S = distance between supports, w = height of specimen, and a = crack length. In these tests a/w=0.3 and s/w=2.4. Although Eq. (10) was derived for s/w = 3 it is approximately correct for s/w = 2.4, overestimating K_I for static loading by 5% at most. The caustics results are only given up to the time of fracture initiation. Thus from the figure it is seen that the specimen with a blunted crack fractured at t=640μs and that the sharper specimen fractured at t=240μs. Up to the time of initiation for specimen 36, the $K_I^d(t)$ records for both tests are nearly identical demonstrating the repeatability of the test. It is seen from the caustics records that the crack tip does not begin to be loaded until 40 μs after impact, approximately the time it takes for stress waves generated by the impact to reflect from the specimen boundaries to the crack tip. This point is also demostrated in Fig. 4 where it is seen that at 42 μs a caustic is just starting to appear indicating that the crack is being loaded.

It was proposed [17] that if the time to fracture, t_f, is large enough, $t_f > 3\tau$, where τ is the period of oscillation of the specimen, then $K_I^d(t)$ may be calculated from Eq. (10). The critical initiation value of K_{Ic}^d is then assumed to be the value corresponding to the maximum load. The period τ for these specimens was 180μs, or 3τ=540μs. (Using a relation given in [18].) Figure 5 shows that throughout the tests, even for $t > 3\tau$, K_I^d from caustics and from the tup load do not agree. Equivalent results were reported by Kalthoff et al., [19,20], who made more extensive tests with metals and polymers.

Figure 5 also shows that fracture initiation occurs about 60μs prior to the time of peak

load. By studying the crack propagation record it was found that the load began to drop rapidly at the time when the crack had propagated completely through the specimen. Thus the peak load is associated not with fracture initation but with fracture completion.

The energy absorbed by the specimen prior to fracture can be calculated by integrating the load-displacement record up to the time of peak load. In the experiments presented here the energy of the falling weight was large enough so that the weight moved with very nearly constant velocity during impact. As a result, the load-time record, P(t), also corresponds to a load-displacement record. Integration of the record for specimen 36 shows that the energy absorbed by the time of peak load ($300\mu s$) is 25% greater than the energy absorbed at the actual time of fracture ($240\mu s$). For the blunted specimen 34, the relative difference between t_f ($640\mu s$) and the time of peak load ($700\mu s$) is smaller, but the absorbed energy is still overestimated by 10%.

As is clear from the above, calculation of fracture toughness by means of impact load measurements and static analyses results in serious errors. Alternatives to optical techniques require complete determination of the boundary conditions (including supports) and the use of a fully elastodynamic analysis.

5. DYNAMIC CRACK PROPAGATION

5.1. Results.

The crack length a(t), crack tip speed $\dot{a}(t)$, and $K_I^d(t)$ records for a typical test (specimen 34) are given in Figs. 6 and 7. The crack length record is differentiated using the incremental polynomial fit method described in the ASTM Test for Constant-Load-Amplitude Fatigue Crack Growth Rates above 10^{-8} m/cycle (E647-81). To find the velocity at data point $a(t_i)$, a curve $a=C_1+C_2t + C_3t^2$ is least squares fit to points $\{a(t_{i-n}), \ldots a(t_i), \ldots a(t_{i+n})\}$ where n is usually 1,2, or 3. The crack tip velocity is then $a(t_i)=C_2+2C_3t_i$. It is clear that this method cannot be used on the first and last data points; thus a graphical method was used for

those points.

If a(t) is such that different differentiation techniques produce widely different $\dot{a}(t)$ records then the results are subject to interpretation. In Fig. 7 $\dot{a}(t)$ for 5 point (n=2) and 3 point (n=1) fits are compared. It is seen that fitting more points results in more smoothing but the two $\dot{a}(t)$ records differ by less than 5% indicating that $\dot{a}(t)$ is relatively insensitive to differentiation technique.

The smooth velocity record gives confidence in these results because it shows that such records are not as subject to interpretation as are similar results for DCB specimens. As discussed in [21], changes in $\dot{a}$ in DCB specimens may occur on time scales smaller than the measurement interval causing the interpretation of the data to be rather subjective.

Note that the $K_I^d(t)$ and $\dot{a}(t)$ records vary in phase in Fig. 7 demonstrating a strong relation between K_I^d and $\dot{a}$. Cross plotting of the results of Fig. 7 produces the relation between K_{Ic}^d and $\dot{a}$ shown in Fig. 8.

The consistency of the present tests is illustrated in Fig. 9 where $\dot{a}(t)$ and $K_I^d(t)$ are shown for specimens 33 and 34, identical blunted crack tip specimens. Due to a small difference in the initial crack tip conditions the cracks initiated at slightly different times (time difference= 45 μs) and slightly different levels of K_I^d. Even so, the results of the two tests generally agree, demonstrating the reproducability and reliability of these tests. As before, $\dot{a}(t)$ and $K_I^d(t)$ vary in phase.

The effect of the crack tip bluntness on stress intensity factor and velocity history is demonstrated in Figs. 5 and 10 where the results for specimens 34 and 36 are compared. The crack tip diameter was 1.4 mm for specimen 34 and 0.3 mm for specimen 36. Figure 5 demonstrates that by increasing the crack bluntness the average crack velocity is increased. Similarly Fig. 10 demonstrates that higher levels of K_I^d may be obtained by blunting the crack. Generally the specimens containing sharp initial crack tips fractured with velocities in the range of 600-800 m/s. To cover a higher velocity range the blunted

specimens were tested, fracturing with velocities of 800-1200 m/s.

5.2. K_I^d versus $\dot{a}$ Relation.

The relation between K_{Ic}^d and $\dot{a}$ for a single experiment (specimen 34) is shown in Fig. 8. Figure 8 suggests a clear dependence of K_{Ic}^d on crack tip velocity. The repeatability of such a result for different load and velocity histories is necessary for assuming that the dynamic fracture toughness depends on velocity through a relation which is purely a material property as is usually assumed for the right hand side of Eq. (1).

Repeatability is indeed demonstrated in the results of Fig. 11. This figure displays the collective results from the present experiments. These results, which correspond to a variety of velocity histories, follow a definite trend. Superimposed are the results from [10] obtained from experiments performed on DCB specimens of the same material and heat treatment. The data point corresponding to specimen 32 ($\dot{a}$=0) is the value of steady state crack propagation toughness obtained from a quasistatic test.

Although this heat treatment of 4340 steel fractures under nominally elastic conditions, the fracture mechanism is ductile hole growth and coalescence. Such conditions were simulated by the analysis of dynamic crack growth given in [2] where the existence of a K_{Ic}^d vs. $\dot{a}$ relationship is demonstrated. Despite greater scatter, for the reasons explained below, experiments performed on double cantiliever beam specimens of a similar 4340 steel [5,9] produced K_{Ic}^d versus $\dot{a}$ relations qualitatively similar to the results obtained here. This agreement of results from different sources and specimen configurations provides strong evidence for the existence of a unique $K_{Ic}^d(\dot{a})$ relationship for this steel. However, for materials that fracture in a truly brittle manner where the micromechanism of fracture is pure cleavage, the results of [2] do not necessarily apply and the existence of a $K_{Ic}^d(\dot{a})$ relationship can be questioned [8].

5.3. Comparison with DCB Tests.

Most of the previous dynamic crack propagation tests in metals were performed with compact tension or double cantilever beam (DCB) specimens [5,9,10,22]. The DCB specimen was often chosen for its relative ease of analysis by means of a dynamic beam model. However the small size of most DCB specimens results in undesirable dynamic effects. Due to the closeness of the specimen boundaries to the crack tip, stress waves released when the crack begins to propagate reflect back to the crack tip causing abrupt changes in $\dot{a}(t)$ and $K_I^d(t)$. Visual evidence of such reflected waves is seen in Fig. 12. The surface waves released when the crack initiates reflect back to the crack tip distorting the caustic. The surface wave patterns suggest that body waves, which will affect K_I^d but cannot be detected by photography, are also present. In addition to the optical distortions, the crack length versus time records from such tests may have discontinuities in slope, causing uncertainty in calculating the crack velocity by differentiation of the crack length record.

Further evidence of strong dynamic effects in DCB specimens is given by the results of Kalthoff et al. [22] ,reproduced here in Fig. 13. The figure shows the K_I^d versus crack length record for an experiment using caustics performed with a DCB specimen. If such large oscillations in K_I^d as seen in Fig. 13 occur on a time scale shorter than the measurement interval, interpretation of the results is uncertain.

In contrast, the drop weight specimen has fewer undesired dynamic effects. The set of photographs from a drop weight test shown in Fig. 4 shows only outgoing surface waves. Due to the longer lateral dimensions of the 3-point bend specimen, no strong reflected stress waves are seen interacting with the crack tip. In addition the results of Figs. 6, 7, 9, and 10 show smoothly varying $\dot{a}(t)$ and $K_I^d(t)$ records making the interpretation of these results straightforward.

Another advantage of drop weight testing combined with high speed photography is that the time of fracture initiation can be found within $\pm$ 2.5 μs (time between frames = 5 μs). In DCB testing the data recording is triggered by the breaking of a trip wire glued on

the specimen ahead of the crack. Thus data for the first part of propagation and for the initiation are lost. As is seen from Fig. 4, the drop weight experiments combine the crack loading, initiation and propagation in a single test. Thus unlike the DCB specimen no data on crack initiation and on the beginning stages of crack growth are lost.

6. CONCLUSIONS

Strong evidence for the existence of a unique K_{Ic}^{d} vs. $\dot{a}$ relation is given for a particular 4340 steel. The new test configuration used here is designed to minimize dynamic effects and the resulting errors in the interpretation of experiments, thus increasing the confidence in the results.

7. ACKNOWLEDGEMENTS

The support of the Office of Naval Research through contract N00014-85-K-0596 is gratefully acknowledged. The authors would also like to acknowledge the laboratory assistance of Mr. Xiaomin Deng.

8. REFERENCES

1. Freund, L.B., in *Mechanics of Fracture*, ASME-AMD Vol. 19, 1976, p. 105-134.

2. Lam, P.S. and Freund, L.B., *Journal of the Mechanics and Physics of Solids*, Vol. 33, 1985, pp. 153-167.

3. Brickstad, B. *International Journal of Fracture*, Vol. 21, 1983, pp. 177-194.

4. Kanazawa, T., Machida, S., Teramoto, T., and Yoshinari, H., *Experimental Mechanics*, Vol. 38 1981, pp. 78-88.

5. Bilek, Z., in *Crack Arrest Methodology and Applications, ASTM STP 711*, American Society for Testing and Materials, 1980, pp. 240-247.

6. Beinert, J., Kalthoff, J.F., in *Mechanics of Fracture,* Vol. VII, G. Sih (ed.), Sijthoff and Noordhoff, 1981, pp. 281-330.

7. Dally, J.W., in *Optical Methods in Mechanics of Solids,* A. Lagarde ed., Sijthoff and Noordhoff, 1980, p. 692.

8. Ravi-Chandar, K. and Knauss, W.G., *International Journal of Fracture,* Vol. 25, 1984, pp. 247-262; Vol. 26, 1984, pp. 65-80, pp. 141-154, pp. 193-204.

9. Kobayashi, T., and Dally, J.W., in *Crack Arrest Methodology and Applications, ASTM STP 711,* American Society for Testing and Materials, 1980, pp. 189-210.

10. Rosakis, A.J., Duffy, J., and Freund, L.B., *Journal of the Mechanics and Physics of Solids,* Vol. 32, 1984, pp. 443-460.

11. Rosakis, A.J., Duffy, J., and Freund, L.B., in *Proceedings, "Workshop on Dynamic Fracture,"* W.G. Knauss et al., eds. California Institute of Technology, 1983, pp. 100-118.

12. Manogg, P., "Anwendungen der Schattenoptik zur Untersuchung des Zerreißvorgags von Platten," Dissertation, Freiburg, Germany, 1964.

13. Rosakis, A.J., and Zehnder, A.T., *Journal of Elasticity,* Vol. 15, 1985, pp. 347-367.

14. Freund, L.B., and Clifton, R.J., *Journal of Elasticity,* Vol. 4, 1974, pp. 293-299.

15. Rosakis, A.J., and Ravi-Chandar, K., *International Journal of Solids and Structures,* Vol. 22, 1986, pp. 121-134.

16. Emery, A.F., Walker, G.E., Williams, J.A., *Journal of Basic Engineering,* Vol. 91, 1969, pp. 618-624.

17. ASTM E 24.03.03, "Proposed Standard Method of Test for Instrumented Impact Testing of Precracked Charpy Specimens of Metallic Materials," Draft 2d, 1981.

18. Ireland, D.R., "Critical Review of Instrumented Impact Testing," Proc. International Conference on Dynamic Fracture Toughness, London, 1976.

19. Kalthoff, J.F., Bohme, W., Winkler, S., and Klemm, W., "Measurements of Dynamic Stress Intensity Factors in Impacted Bend Specimens," CSNI Specialist Meeting on Instrumented Precracked Charpy Testing, Electric Power Research Institute, Palo Alto, CA, 1980.

20. Kalthoff, J.F., Winkler, S., Klemm, W., and Beinert, J., "On the Validity of K_{Id}-Measurements in Instrumented Impact Tests," Proceedings, 5th International Conference on Structural Mechanics in Reactor Technology, Berlin, 1979, G 4/5.

21. Rosakis, A.J., and Zehnder, A.T., *International Journal of Fracture*, Vol. 27, 1985, pp. 169-186.

22. Kalthoff, J.F., Beinert, J., Winkler, S., and Klemm, W., in *Crack Arrest Methodolgy and Applications, ASTM STP 711*, American Society for Testing and Materials, 1980, pp. 109-127.

9. FIGURE CAPTIONS

Figure 1. Formation of caustic due to reflection of light from the polished, deformed specimen surface near the crack tip.

Figure 2. Static stress intensity factor as determined by caustics, divided by plane stress value versus distance r from the crack tip (from Rosakis and Ravi-Chandar [15]).

Figure 3. Specimen and experimental setup for high speed photography of caustics.

Figure 4. Selected photographs showing loading, initiation, and propagation stages of crack growths in a 3-point bend specimen.

Figure 5. Stress intensity factor prior to crack initiation. Both K_I^d calculated from caustics and from the tup load are given. Specimen 34, crack tip diameter ϕ =1.4 mm; specimen 36, ϕ = 0.3 mm.

Figure 6. Crack length versus time. Specimen 34, crack tip diameter ϕ =1.4 mm; specimen 36, ϕ =0.3 mm.

Figure 7. Specimen 34, stress intensity factor and crack speed records. K_I^d and $\dot{a}$ vary in phase.

Figure 8. Resulting $K_{Ic}^d(\dot{a})$ relation for specimen 34.

Figure 9. Stress intensity factor and crack speed for identical specimens. Note consistency of results.

Figure 10. Effect of crack tip bluntness on K_I^d. Blunted specimen 34 has higher K_I^d than sharper specimen 36.

Figure 11. Dynamic fracture toughness K_{Ic}^d versus crack speed $\dot{a}$. Collected data from impact testing are presented with equivalent results from DCB specimens of the same material.

Figure 12. Dynamic crack growth in a DCB specimen. Strong dynamic effects are demonstrated by unloading waves emitted from crack tip and reflected from specimen boundaries.

Figure 13. Stress intensity factor versus crack length for a DCB test. K_{IQ} = stress intensity factor for initiation from an initially blunted crack (from Kalthoff et al., [22]).

Table 1. Material Properties 4340 Steel,
Aircraft Quality, Vacuum Degassed

Chemical Composition, %

C	Mn	P	S	Si	Ni	Cr	Mo	Cu	Fe
.39	.72	.015	.011	.21	1.87	.83	.25	.12	balance

Heat Treatment : 843°C 1 1/2 hour, oil quench
315°C 1 hour, oil cool.

Material Properties : Hardness = 50 HRC
Tensile Strength = 1490 MPa
Fracture Initiation Toughness, K_{Ic} = 47 MPa$\sqrt{m}$
Quasi-Static Propagation Toughness, K_I' = 62 MPa$\sqrt{m}$

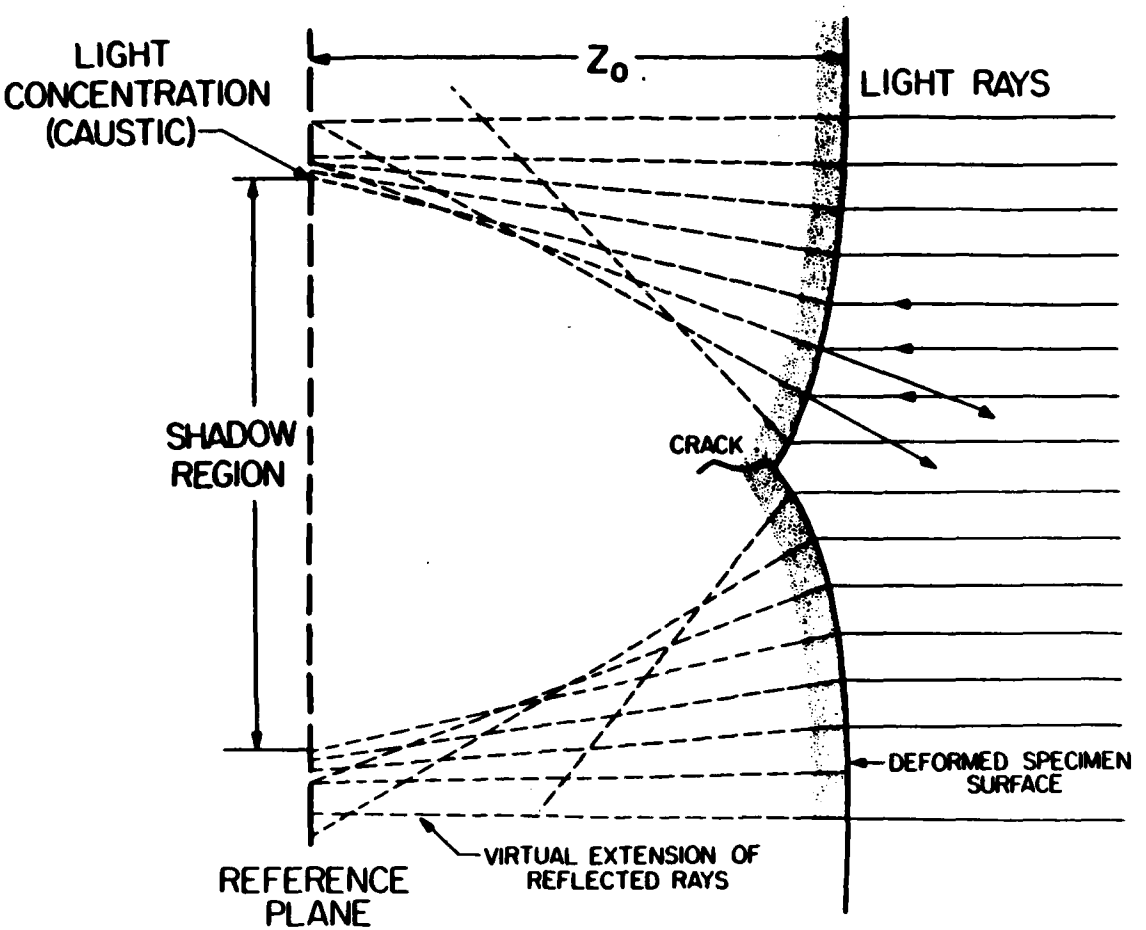

Figure 1. Formation of caustic due to reflection of light from the polished, deformed specimen surface near the crack tip.

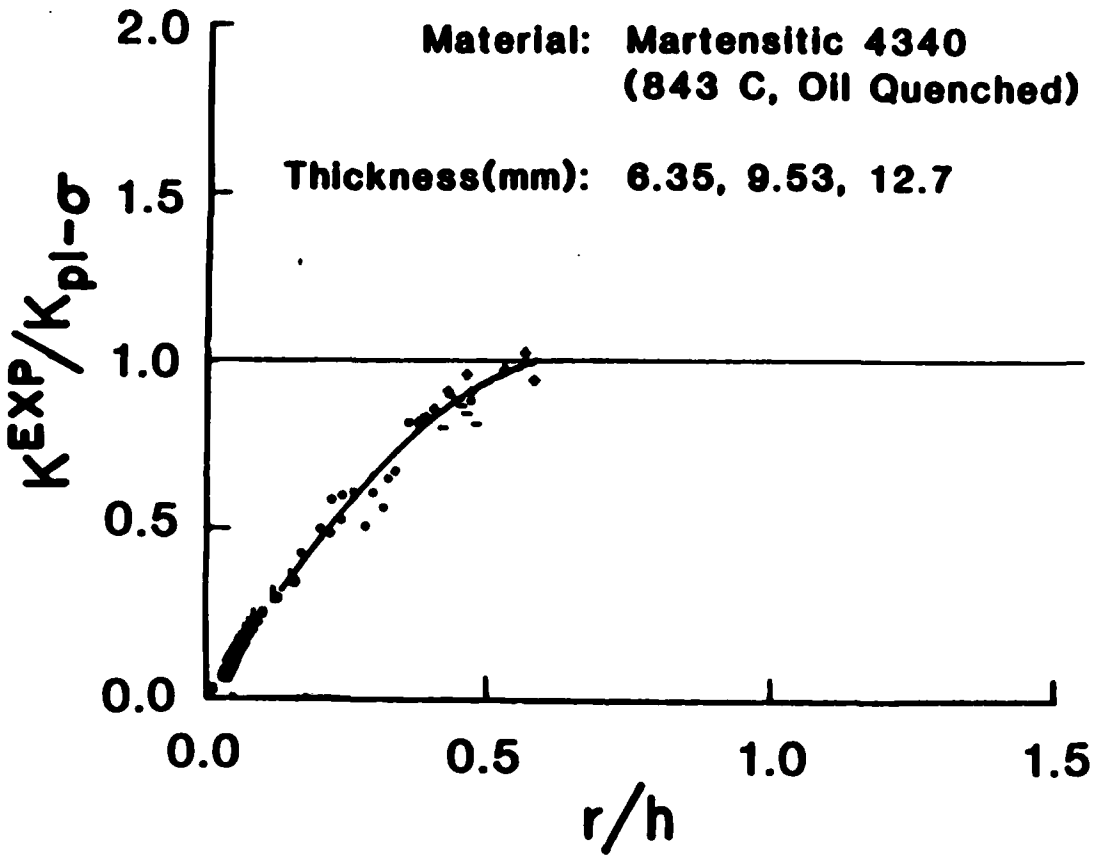

Figure 2. Static stress intensity factor as determined by caustics, divided by plane stress value versus distance r from the crack tip (from Rosakis and Ravi-Chandar [15]).

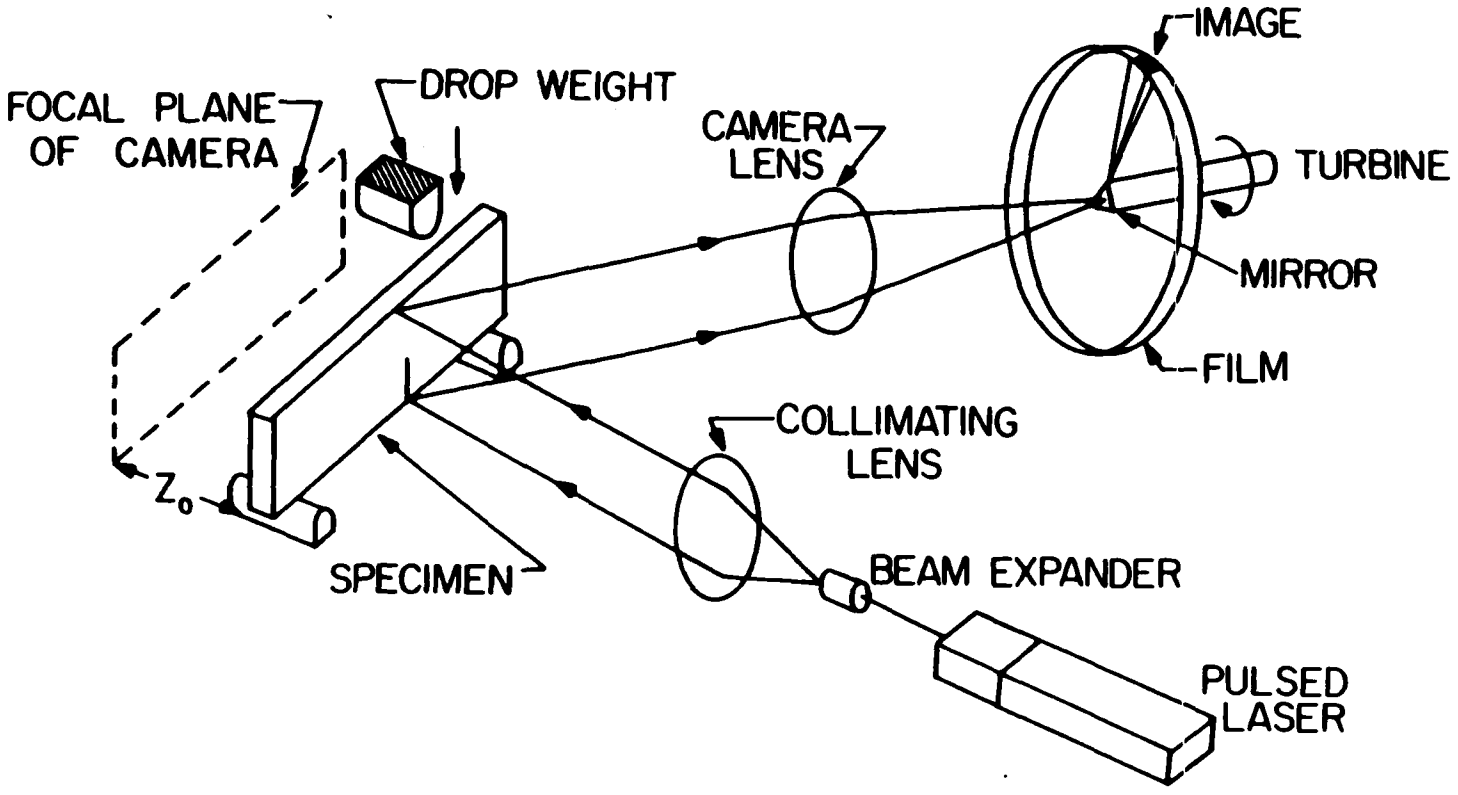

Figure 3. Specimen and experimental setup for high speed photography of caustics.

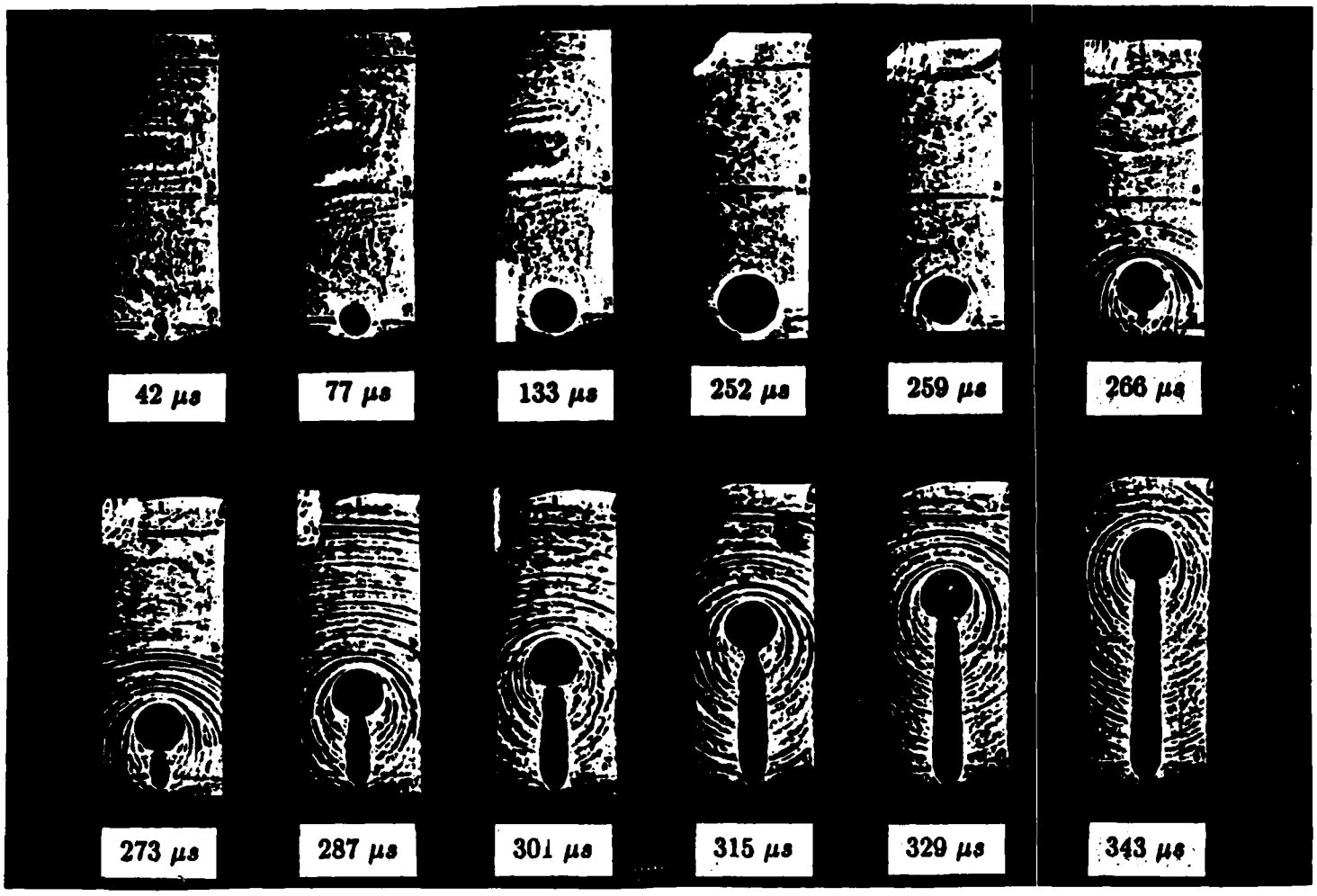

Figure 4. Selected photographs showing loading, initiation, and propagation stages of crack growths in a 3-point bend specimen.

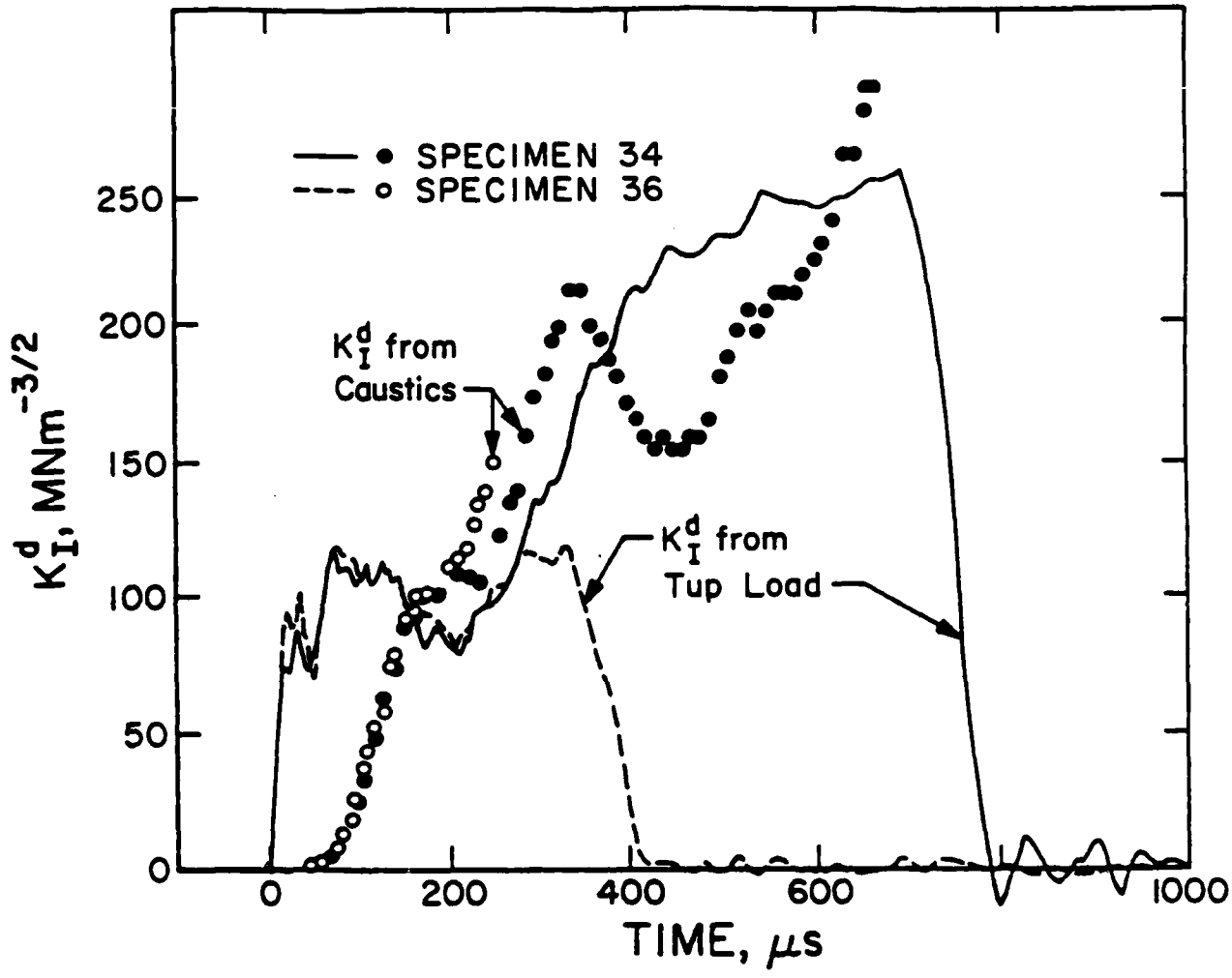

Figure 5. Stress intensity factor prior to crack initiation. Both K_I^d calculated from caustics and from the tup load are given. Specimen 34, crack tip diameter ϕ = 1.4 mm; specimen 36, ϕ = 0.3 mm.

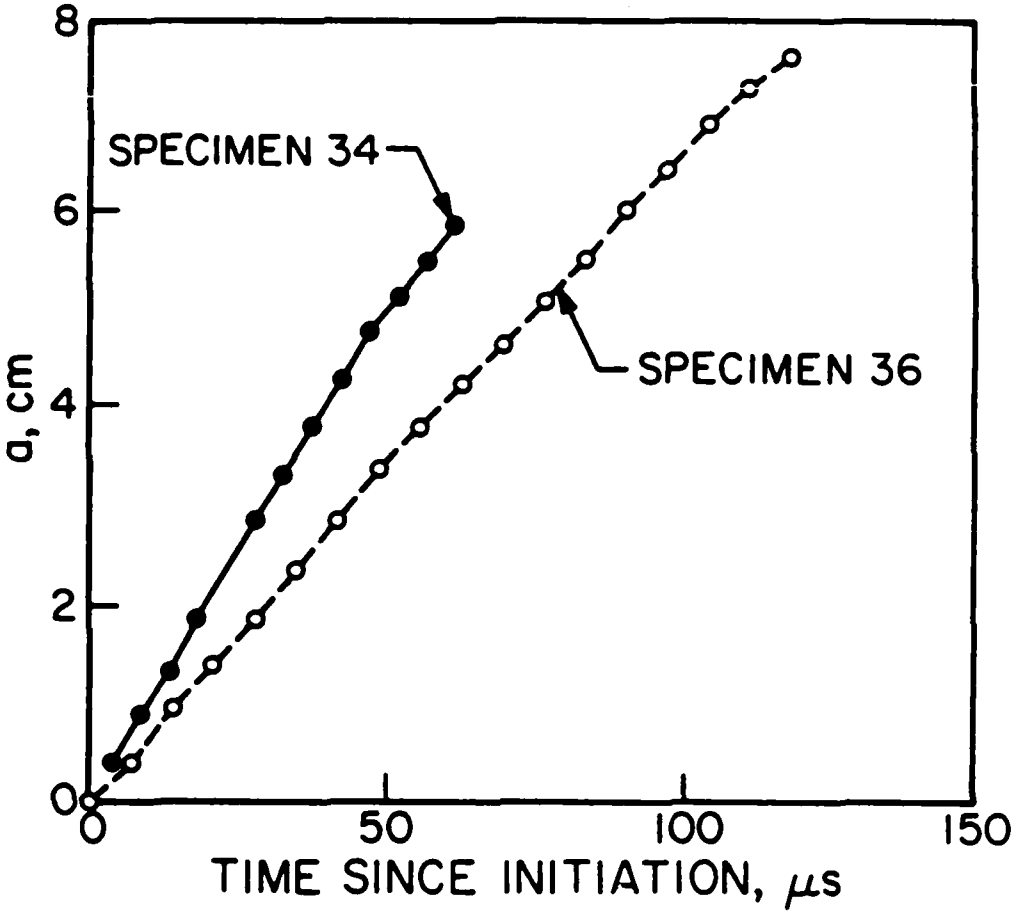

Figure 6. Crack length versus time. Specimen 34, crack tip diameter ϕ =1.4 mm; specimen 36, ϕ =0.3 mm.

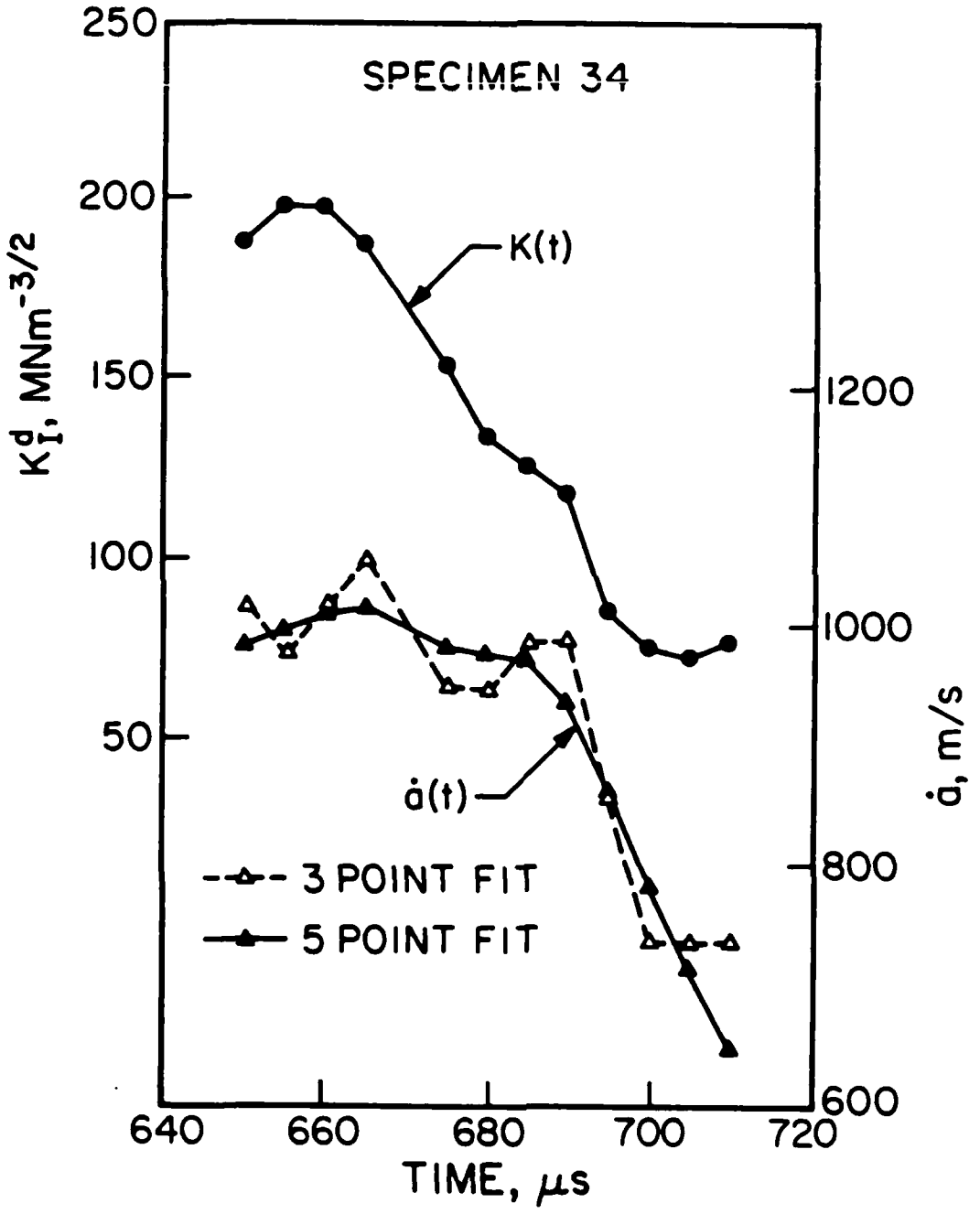

Figure 7. Specimen 34, stress intensity factor and crack speed records. K_I^d and $\dot{a}$ vary in phase.

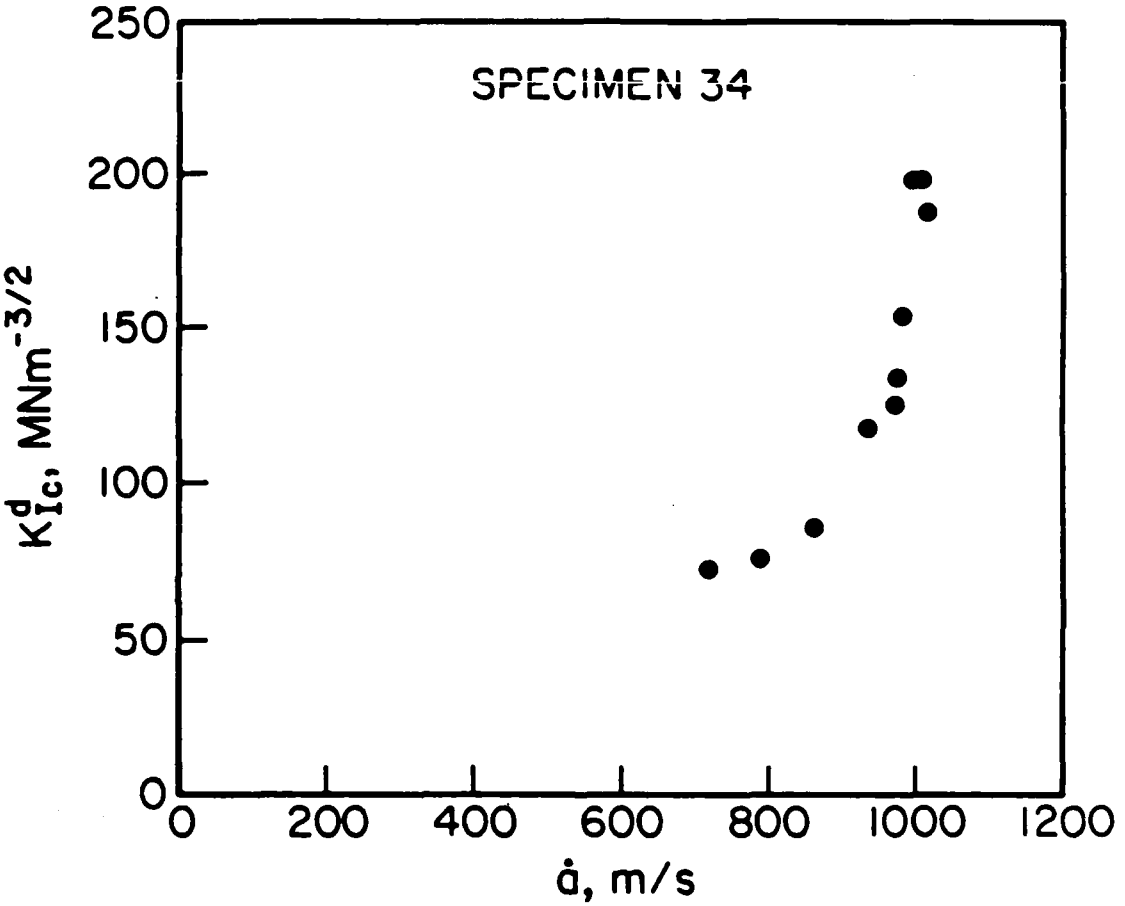

Figure 8. Resulting $K^d_{Ic}(\dot{a})$ relation for specimen 34.

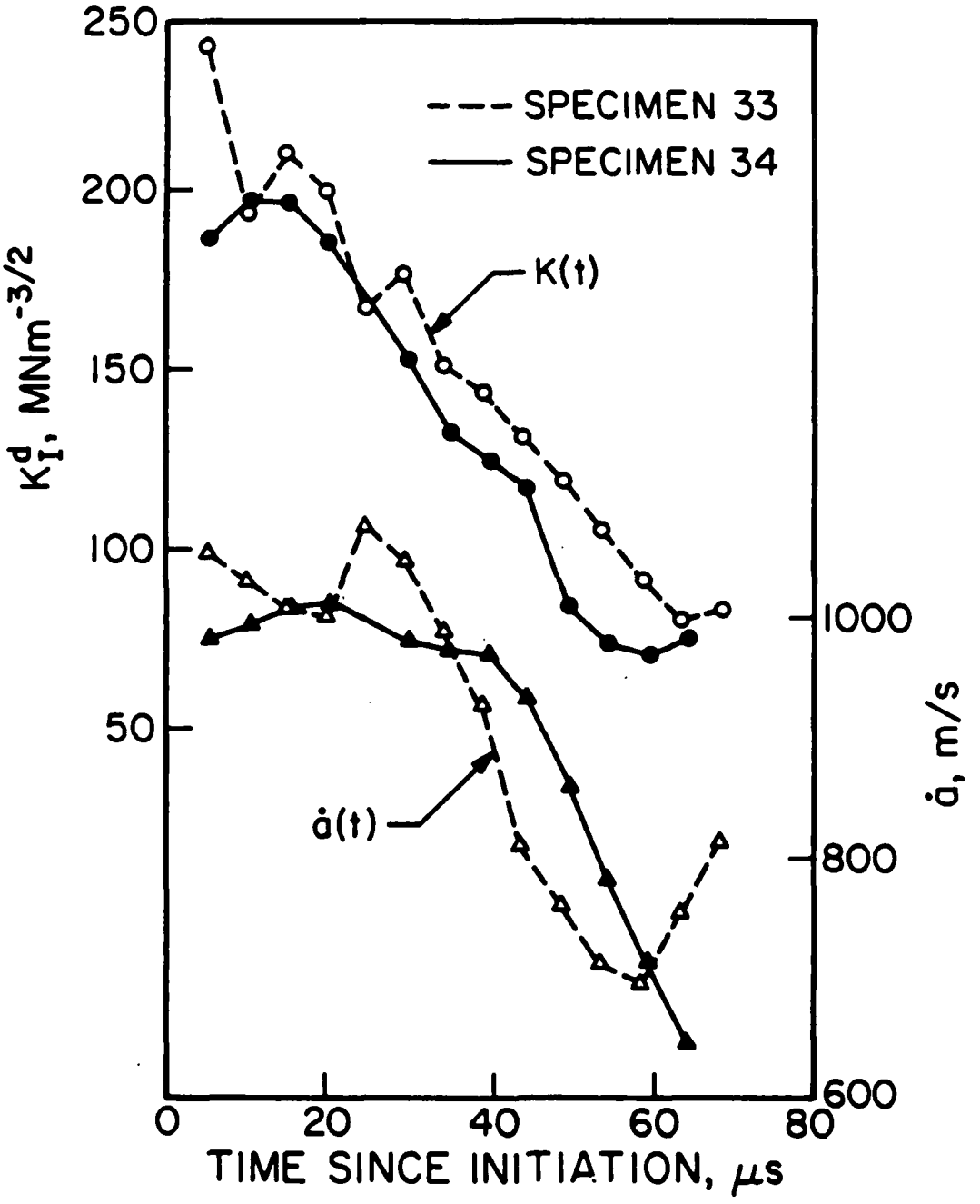

Figure 9. Stress intensity factor and crack speed for identical specimens. Note consistency of results.

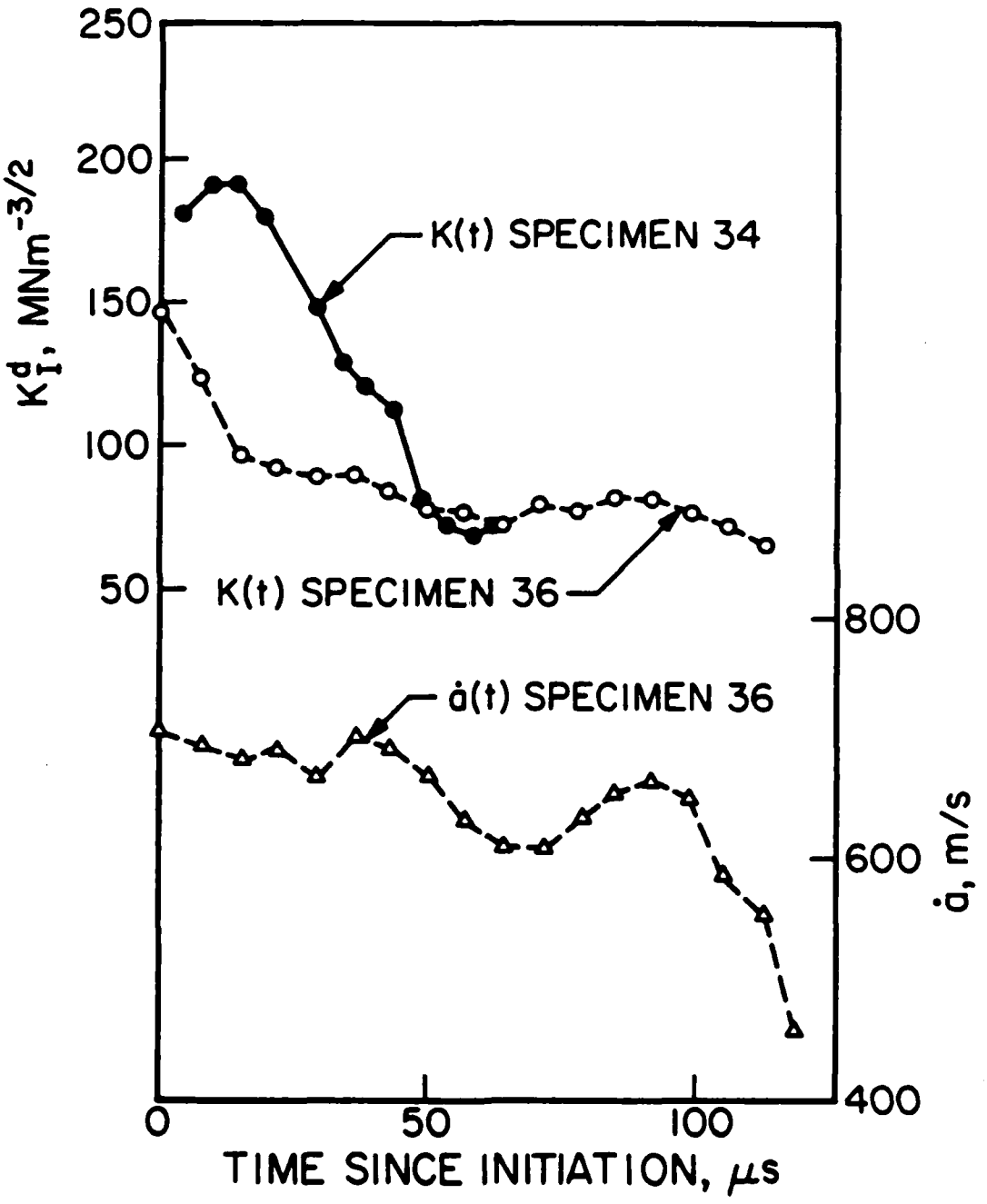

Figure 10. Effect of crack tip bluntness on K_I^d. Blunted specimen 34 has higher K_I^d than sharper specimen 36.

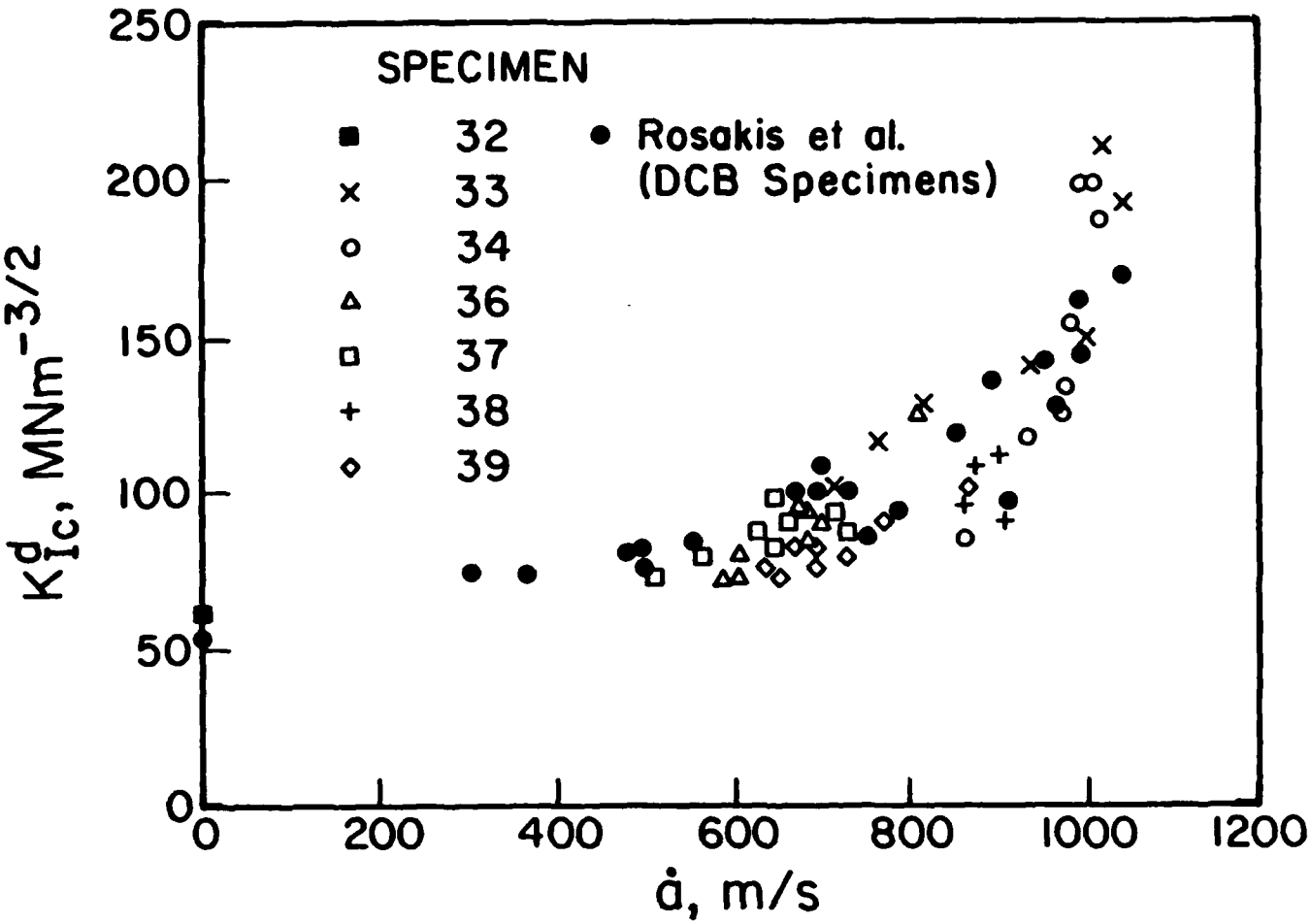

Figure 11. Dynamic fracture toughness K_{Ic}^{d} versus crack speed $\dot{a}$. Collected data from impact testing are presented with equivalent results from DCB specimens of the same material.

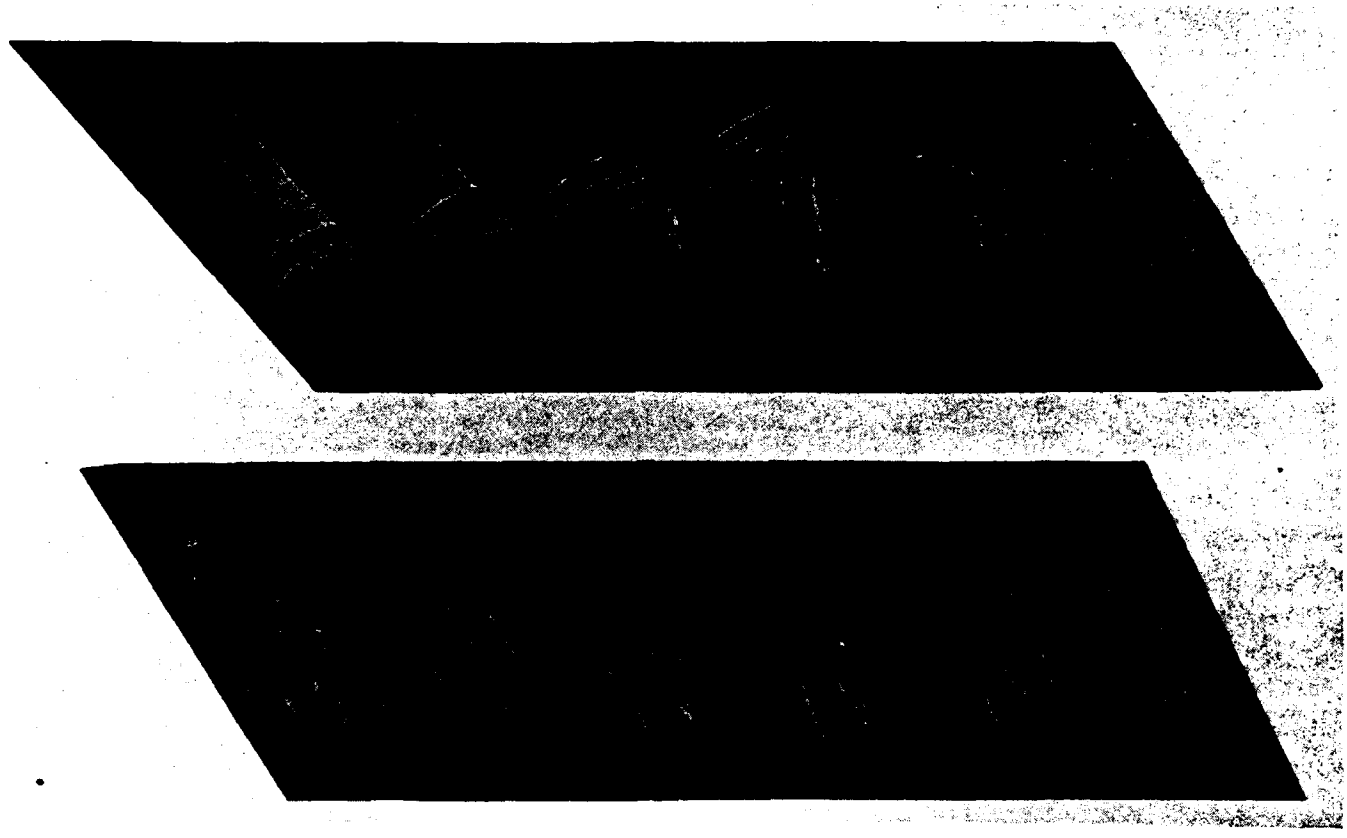

Figure 12. Dynamic crack growth in a DCB specimen. Strong dynamic effects are demonstrated by unloading waves emitted from crack tip and reflected from specimen boundaries.

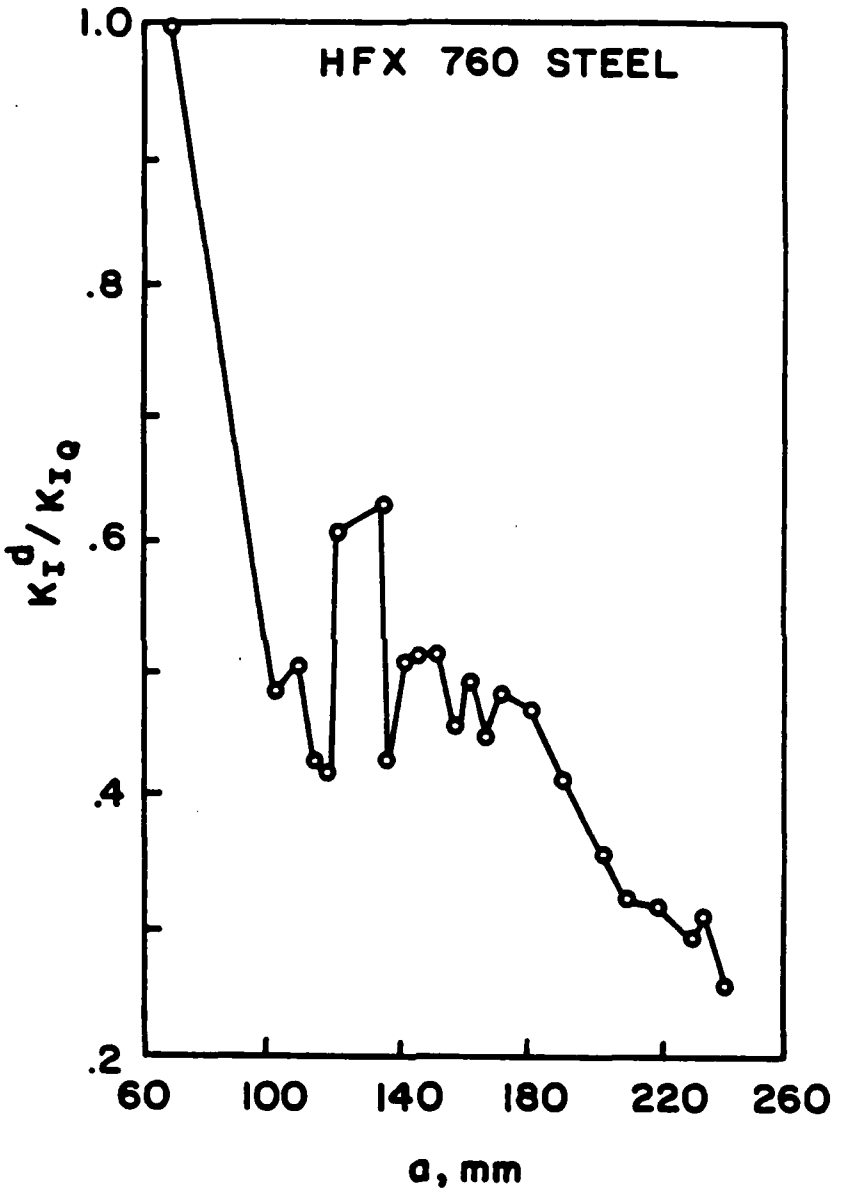

Figure 13. Stress intensity factor versus crack length for a DCB test. K_{IQ} = stress intensity factor for initiation from an initially blunted crack (from Kalthoff et al., [22]).

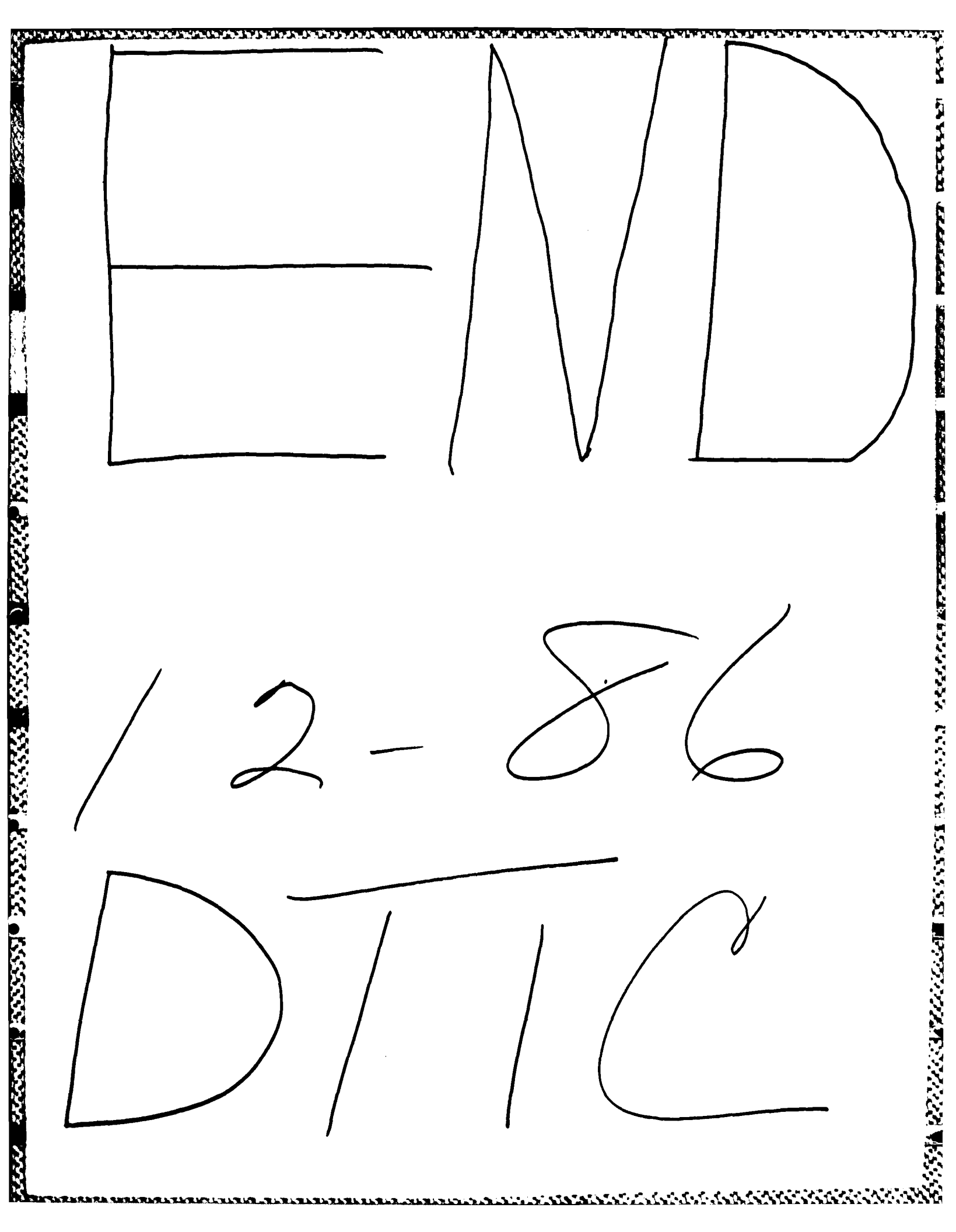
END
12-86
DTIC